Methods

Cell culture. Bruce 4 C57BL/6 mESCs (Merk Millipore, Billerica, MA) (and later derivatives) were cultured in 2i conditions (StemSure D-MEM [Wako Pure Chemicals, Osaka, Japan], 15% fetal bovine serum, 0.1 mM β-mercaptoethanol, 1 × MEM nonessential amino acids [Wako Pure Chemicals], 2 mM L-alanyl-L-glutamine solution [Wako Pure Chemicals], 1000 U/mL LIF [Wako Pure Chemicals], 20 μg/mL gentamicin [Wako Pure Chemicals], 3 μM CHIR99021, and 1 μM PD0325901) on a 0.1% gelatin-coated dish. Before each experiment, cells were passaged two times and cultured in 2i conditions as well as serum conditions (StemSure D-MEM, 15% fetal bovine serum, 0.1 mM β-mercaptoethanol, 1 × MEM nonessential amino acids, 2 mM L-alanyl-L-glutamine solution, 1000 U/mL LIF, 20 μg/mL gentamicin), or in serum conditions containing 2i inhibitors or PD0325901 at several concentrations, as described in Supplementary Table S1. TSA and 5-AzaC were added to the cells at a final concentration of 50 nM and 50 μM, respectively. They were applied for 72 hours.

Plasmid construction. TALEN expression vectors were constructed as described in Ochiai et al[20]. A part of the vector was derived from pTALEN_v2 (NG) vector (plasmid 32190, Addgene, Cambridge, MA)[47]. The TALEN target sequences and their amino acid sequences are described in Figure 1b and Supplementary Figure S7, respectively. Targeting vectors containing either 2A-loxP-hsvTK-2A-Puro-loxP-24×MS2 (pTV-mNanog-PMS) or 2A-loxP-hsvTK-2A-Hyg-loxP-24×PP7 (pTV-mNanog-HPP) were constructed by polymerase chain reaction (PCR) and standard cloning techniques. The 24× MS2 and 24× PP7 sites in the targeting vectors were derived from pCR4-24XMS2SL-stable (Addgene plasmid 31865) and the pCR4-24XPP7SL (Addgene plasmid 31864), respectively[14,48]. The hsvTK in the targeting vector was derived from the pLOX-TERT-iresTK vector (Addgene plasmid 12245)[49]. The nucleotide sequences of the targeting vectors are provided in Supplementary Figure S8 and S9. To construct pPB-LR5-CAG-MCP-mNeonGreen-IRES-Neo, the CAG-MCP-mNeonGreen-IRES-Neo cassette was inserted into the NheI/XhoI site of pPB-LR5[50]. The cDNA of MCP in pPB-LR5-CAG-MCP-mNeonGreen-IRES-Neo was derived from the phage-ubc-nls-ha-tdMCP-gfp vector (Addgene plasmid 40649)[51].

Gene targeting. To generate $Nanog^{MS2/MS2}$ cells, C57BL/6 mESCs (0.5×10^5) were plated in 24-well plates the day before transfection. The next day, the cells were transfected with 1 μg of pTV-mNanog-PMS and 250 ng each of TALEN expression vectors using Lipofectamine 2000 (Life Technologies, Gaithersburg, MD) according to the manufacturer's instructions. After 24 h, the cells were transferred to 10-cm plates, incubated for 72 h, and then subjected to puromycin selection (1 μg/mL). Homologous recombination was verified by PCR and Southern blotting. Then, to excise the selection cassette flanked by loxP sites, 500 ng of Cre expression vector (pCAG-Cre) (Addgene plasmid 13775)[52] was transfected into the obtained clone ($Nanog^{TP\text{-}MS2/TP\text{-}MS2}$). The genotype of the resultant ganciclovir-resistant ESC ($Nanog^{MS2/MS2}$, NM clone) was confirmed by Southern blotting. For constitutive expression of NLS-MCP-mNeonGreen, pPB-LR5-CAG-MCP-mNeonGreen-IRES-Neo plasmid was transfected with pCMV-hyPBase[53] into NM cells, and G418-resistant clones were obtained. To generate $Nanog^{PP7/MS2}$ (NMP cells), 1 μg of pTV-mNanog-HPP was transfected with 250 ng of TALEN expression vectors into C57BL/6 ESCs, as described above. The resultant hygromycin-resistant clone ($Nanog^{TH\text{-}PP7/+}$) was subsequently subjected to a second targeting with pTV-mNanog-PMS and TALEN expression vectors. The resultant puromycin-resistant clone ($Nanog^{TH\text{-}PP7/+}$) was subsequently subjected to a second targeting with pTV-mNanog-PMS and TALEN expression vectors. The genotype of the resultant puromycin-resistant mESC ($Nanog^{TH\text{-}PP7/TP\text{-}MS2}$) was confirmed by Southern blot. Then, to excise the selection cassette flanked by loxP sites, pCAG-Cre was transfected into the obtained clone ($Nanog^{TH\text{-}PP7/TP\text{-}MS2}$). The genotype of the resultant ganciclovir-resistant NMP cell was confirmed by Southern blot. Southern blots were performed as described previously[20].

Immunostaining. Immunostaining was performed on fixed cells (4% paraformaldehyde in BBS [50 mM BES, 280 mM NaCl, 1.5 mM $Na_2HPO_4{\cdot}2H_2O$] with 1 mM $CaCl_2$, for 15 min), washed, and blocked for 30 min in BBT-BSA buffer (BBS with 0.5% BSA, 0.1% Triton, and 1 mM $CaCl_2$). Cells with primary antibodies were incubated overnight at 4°C at the following dilutions: anti-Nanog (1 : 500; MLC-51, eBioscience, San Diego, CA), anti-Oct4 (1 : 500; ab19857, Abcam, Cambridge, MA), anti-SSEA-1 (1 : 250, ab16285, Abcam). Cells were washed and blocked in BBT-BSA and then incubated with Hoechst33342 (1 : 1000, Life Technologies) and Alexa-conjugated secondary antibodies (1 : 500, Life Technologies). Images were acquired using an Olympus IX83 microscope (Olympus, Tokyo, Japan) with a CSU-W1 confocal unit (Yokogawa, Tokyo, Japan).

smFISH. Trypsinized cells were transferred onto Laminin-511 (BioLamina, Stockholm, Sweden)-coated round coverslips and cultured for 1 h at 37°C and 5% CO_2. Cells were washed with phosphate-buffered saline (PBS), fixed with 4% paraformaldehyde in PBS for 10 min, and washed with PBS two times. Then, cells were permeabilized in 70% ethanol at 4°C overnight. Following a wash with 10% formamide dissolved in 2× SSC, the cells were hybridized to probe sets in 60 μL of hybridization buffer containing 2× SSC, 10% dextran sulfate, 10% formamide, and each probe set. Hybridization was performed for 4 h at 37°C in a moist chamber. The coverslips were washed with 10% formamide in 2× SSC solution, and then with 10% formamide in 2× SSC solution with Hoechst33342 (1 : 1000). Hybridized cells were mounted in catalase/glucose oxidase containing mounting media, as described previously[54]. Images were acquired using an Olympus IX83 microscope with a CSU-W1 confocal unit, a 100× Olympus oil immersion objective of 1.40 NA, and an iXon3 EMCCD camera (Andor, Belfast, UK), with laser illumination at 405 nm, 561 nm, and 637 nm, and were analyzed using Metamorph software (Universal Imaging Corporation, West Chester, PA); 101 z planes per site spanning 15 μm were acquired. Images were filtered with a one-pixel diameter 3D median filter and subjected to background subtraction via a rolling ball radius of 5 pixels, using ImageJ software. Detection and counting of smFISH signals were performed using Imaris software (Bitmap, Zurich, Switzerland) as described by Yunger et al[55]. Mixtures of *Nanog* exonic and intronic probes conjugated with CAL Fluor Red 590 were obtained from BioSearch Inc (Novato, CA) and used at 0.25 μM. MS2 probes conjugated with Cy5, and PP7 probes conjugated with Cy3 were obtained from Operon Technologies Inc. (Alameda, CA) and used at 0.52 μM each. Probe sequences are shown in Supplementary Table S2. To estimate mRNA half-life, NM and C57BL6 mESCs were cultured in 2i medium containing actinomycin D (5 μg/ml) for 0, 2, 4, and 6 hours, and subjected to smFISH analysis using *Nanog* exonic probes.

smFISH-immunostaining. Trypsinized cells were transferred onto μ-Slide 8-well (Ibidi, Martinsried, Germany) coated with Laminin-511 and cultured for 1 h at 37°C and 5% CO_2. Then, cells were fixed and subjected to smFISH as described above using *Nanog* exonic probes. After the image acquisition, cells were subjected to immunostaining, as described in the immunostaining section above, using the anti-Nanog antibody and Alexa Fluor 647 goat anti-rat IgG (H+L) (1 : 500, Life Technologies). The images were acquired using an Olympus IX83 microscope with a CSU-W1 confocal unit, 60× Olympus oil-immersion objective of 1.42 NA; 101 z planes per site, spanning 15 μm, were analyzed. smFISH images were filtered using ImageJ, with a one-pixel diameter 3D median filter, and subjected to background subtraction via a rolling ball radius of 2 pixels. Further fluorescence subtraction (100, 16-bit pixel unit) for almost complete removal of background intensity and maximum-intensity projection was subsequently performed. Immunostained images were filtered with a two-pixel diameter 3D median filter, and subjected to fluorescence subtraction (300, 16-bit pixel unit) for almost complete removal of background intensity and maximum-intensity projection, using ImageJ. The freehand selection tool of ImageJ was used for measurements of integrated signal intensity in each cell.

Live imaging. Trypsinized cells were transferred onto μ-Slide 8-well coated with Laminin-511 and cultured overnight at 37°C and 5% CO_2. The next day, after the medium was changed, cells were subjected to live imaging by an Olympus IX83 microscope with a CSU-W1 confocal unit and a 60× Olympus oil-immersion objective of 1.42 NA for quantification of transcriptional dynamics. Fluorescence images were captured using an iXon3 EMCCD camera, equipped with a 488-nm laser, a stage-top microscope incubator (5% CO_2 at 37°C; Tokai Hit, Shizuoka, Japan), and an ASI MS-2000 piezo stage (ASI, Lyon, France), and were analyzed using Metamorph software; 41 z planes per site, spanning 12 μm, were acquired with a 2-min interval time for 4 h. Acquired images were filtered with a one-pixel diameter 3D median filter using ImageJ. Detection of fluorescent spots was performed using the "Spot" function in Imaris with a spot diameter set at 0.75 μm (semi-automatic detection). For observation of individual mRNA spots, a 100× Olympus oil-immersion objective of 1.40 NA was used. See Supplementary Video S3 and Figure S3 for details.

1. Mitsui, K. *et al.* The homeoprotein Nanog is required for maintenance of pluripotency in mouse epiblast and ES cells. *Cell* **113**, 631–642 (2003).
2. Chambers, I. *et al.* Nanog safeguards pluripotency and mediates germline development. *Nature* **450**, 1230–1234 (2007).
3. Kalmar, T. *et al.* Regulated Fluctuations in Nanog Expression Mediate Cell Fate Decisions in Embryonic Stem Cells. *PLoS Biol* **7**, e1000149 (2009).
4. Torres-Padilla, M. E. & Chambers, I. Transcription factor heterogeneity in pluripotent stem cells: a stochastic advantage. *Development* **141**, 2173–2181 (2014).
5. Nichols, J., Silva, J., Roode, M. & Smith, A. Suppression of Erk signalling promotes ground state pluripotency in the mouse embryo. *Development* **136**, 3215–3222 (2009).
6. Wray, J., Kalkan, T. & Smith, A. G. The ground state of pluripotency. *Biochem. Soc. Trans.* **38**, 1027–1032 (2010).
7. Herberg, M., Kalkan, T., Glauche, I., Smith, A. & Roeder, I. A Model-Based Analysis of Culture-Dependent Phenotypes of mESCs. *PLoS ONE* **9**, e92496 (2014).
8. Festuccia, N. *et al.* Esrrb is a direct Nanog target gene that can substitute for Nanog function in pluripotent cells. *Cell Stem Cell* **11**, 477–490 (2012).
9. Navarro, P. *et al.* OCT4/SOX2-independent Nanog autorepression modulates heterogeneous Nanog gene expression in mouse ES cells. *EMBO J* **31**, 4547–4562 (2012).
10. Miyanari, Y. & Torres-Padilla, M.-E. Control of ground-state pluripotency by allelic regulation of Nanog. *Nature* **483**, 470–473 (2012).
11. Hansen, C. H. & van Oudenaarden, A. Allele-specific detection of single mRNA molecules in situ. *Nat Methods* **10**, 869–871 (2013).
12. Elowitz, M. B., Levine, A. J., Siggia, E. D. & Swain, P. S. Stochastic gene expression in a single cell. *Science* **297**, 1183–1186 (2002).

13. Raser, J. M. & O'Shea, E. K. Control of stochasticity in eukaryotic gene expression. *Science* **304**, 1811–1814 (2004).
14. Bertrand, E. *et al.* Localization of ASH1 mRNA particles in living yeast. *Mol Cell* **2**, 437–445 (1998).
15. Lionnet, T. & Singer, R. H. Transcription goes digital. *EMBO Rep* **13**, 313–321 (2012).
16. Janicki, S. M. *et al.* From silencing to gene expression: real-time analysis in single cells. *Cell* **116**, 683–698 (2004).
17. Chubb, J. R., Trcek, T., Shenoy, S. M. & Singer, R. H. Transcriptional pulsing of a developmental gene. *Curr Biol* **16**, 1018–1025 (2006).
18. Lionnet, T. *et al.* A transgenic mouse for in vivo detection of endogenous labeled mRNA. *Nat Methods* **8**, 165–170 (2011).
19. Sakuma, T. *et al.* Repeating pattern of non-RVD variations in DNA-binding modules enhances TALEN activity. *Sci Rep* **3**, 3379 (2013).
20. Ochiai, H. *et al.* TALEN-mediated single-base-pair editing identification of an intergenic mutation upstream of BUB1B as causative of PCS (MVA) syndrome. *Proc Natl Acad Sci USA* **111**, 1461–1466 (2014).
21. Raj, A., van den Bogaard, P., Rifkin, S. A., van Oudenaarden, A. & Tyagi, S. Imaging individual mRNA molecules using multiple singly labeled probes. *Nat Methods* **5**, 877–879 (2008).
22. Ambrosetti, D. C., Basilico, C. & Dailey, L. Synergistic activation of the fibroblast growth factor 4 enhancer by Sox2 and Oct-3 depends on protein-protein interactions facilitated by a specific spatial arrangement of factor binding sites. *Mol Cell Biol* **17**, 6321–6329 (1997).
23. Kunath, T. *et al.* FGF stimulation of the Erk1/2 signalling cascade triggers transition of pluripotent embryonic stem cells from self-renewal to lineage commitment. *Development* **134**, 2895–2902 (2007).
24. Herberg, M., Kalkan, T., Glauche, I., Smith, A. & Roeder, I. A model-based analysis of culture-dependent phenotypes of mESCs. *PLoS ONE* **9**, e92496 (2014).
25. Jonkers, I., Kwak, H. & Lis, J. T. Genome-wide dynamics of Pol II elongation and its interplay with promoter proximal pausing, chromatin, and exons. *eLife* **3**, e02407 (2014).
26. Muramoto, T. *et al.* Live imaging of nascent RNA dynamics reveals distinct types of transcriptional pulse regulation. *Proc Natl Acad Sci USA* **109**, 7350–7355 (2012).
27. Larson, D. R. *et al.* Direct observation of frequency modulated transcription in single cells using light activation. *eLife* **2**, e00750–e00750 (2013).
28. Singer, Z. S. *et al.* Dynamic Heterogeneity and DNA Methylation in Embryonic Stem Cells. *Mol Cell* **55**, 319–331 (2014).
29. Peccoud, J. & Ycart, B. Markovian modeling of gene-product synthesis. *Theoretical population biology* **48**, 222–234 (1995).
30. Raj, A., Peskin, C. S., Tranchina, D., Vargas, D. Y. & Tyagi, S. Stochastic mRNA synthesis in mammalian cells. *PLoS Biol* **4**, e309 (2006).
31. Larson, D. R., Singer, R. H. & Zenklusen, D. A single molecule view of gene expression. *Trends Cell Biol.* **19**, 630–637 (2009).
32. Hocine, S., Raymond, P., Zenklusen, D., Chao, J. A. & Singer, R. H. Single-molecule analysis of gene expression using two-color RNA labeling in live yeast. *Nat Methods* **10**, 119–121 (2012).
33. Swain, P. S., Elowitz, M. B. & Siggia, E. D. Intrinsic and extrinsic contributions to stochasticity in gene expression. *Proc Natl Acad Sci USA* **99**, 12795–12800 (2002).
34. Yoshida, M., Horinouchi, S. & Beppu, T. Trichostatin A and trapoxin: novel chemical probes for the role of histone acetylation in chromatin structure and function. *Bioessays* **17**, 423–430 (1995).
35. Veselý, J. Mode of action and effects of 5-azacytidine and of its derivatives in eukaryotic cells. *Pharmacol. Ther.* **28**, 227–235 (1985).
36. Dietrich, J.-E. & Hiiragi, T. Stochastic patterning in the mouse pre-implantation embryo. *Development* **134**, 4219–4231 (2007).
37. Abranches, E. *et al.* Stochastic NANOG fluctuations allow mouse embryonic stem cells to explore pluripotency. *Development* **141**, 2770–2779 (2014).
38. Ficz, G. *et al.* FGF signaling inhibition in ESCs drives rapid genome-wide demethylation to the epigenetic ground state of pluripotency. *Cell Stem Cell* **13**, 351–359 (2013).
39. Ohnishi, Y. *et al.* Cell-to-cell expression variability followed by signal reinforcement progressively segregates early mouse lineages. *Nat Cell Biol* **15**, 1–13 (2013).
40. Brown, C. R., Mao, C., Falkovskaia, E., Jurica, M. S. & Boeger, H. Linking Stochastic Fluctuations in Chromatin Structure and Gene Expression. *PLoS Biol* **11**, e1001621 (2013).
41. van Royen, M. E., Zotter, A., Ibrahim, S. M., Geverts, B. & Houtsmuller, A. B. Nuclear proteins: finding and binding target sites in chromatin. *Chromosome Res.* **19**, 83–98 (2011).
42. Wu, C. Y., Feng, X. & Wei, L. N. Coordinated repressive chromatin-remodeling of Oct4 and Nanog genes in RA-induced differentiation of embryonic stem cells involves RIP140. *Nucleic Acids Res* **42**, 4306–4317 (2014).
43. Nagano, T. *et al.* Single-cell Hi-C reveals cell-to-cell variability in chromosome structure. *Nature* **502**, 59–64 (2014).
44. Noordermeer, D. *et al.* Variegated gene expression caused by cell-specific long-range DNA interactions. *Nat Cell Biol* **13**, 944–951 (2011).
45. Apostolou, E. *et al.* Genome-wide chromatin interactions of the Nanog locus in pluripotency, differentiation, and reprogramming. *Cell Stem Cell* **12**, 699–712 (2013).
46. Eckersley-Maslin, M. A. *et al.* Random Monoallelic Gene Expression Increases upon Embryonic Stem Cell Differentiation. *Dev Cell* **28**, 351–365 (2014).
47. Sanjana, N. E. *et al.* A transcription activator-like effector toolbox for genome engineering. *Nat Protoc* **7**, 171–192 (2012).
48. Larson, D. R., Zenklusen, D., Wu, B., Chao, J. A. & Singer, R. H. Real-time observation of transcription initiation and elongation on an endogenous yeast gene. *Science* **332**, 475–478 (2011).
49. Salmon, P. *et al.* Reversible immortalization of human primary cells by lentivector-mediated transfer of specific genes. *Mol Ther* **2**, 404–414 (2000).
50. Yusa, K., Rad, R., Takeda, J. & Bradley, A. Generation of transgene-free induced pluripotent mouse stem cells by the piggyBac transposon. *Nat Methods* **6**, 363–369 (2009).
51. Wu, B., Chao, J. A. & Singer, R. H. Fluorescence fluctuation spectroscopy enables quantitative imaging of single mRNAs in living cells. *Biophysical Journal* **102**, 2936–2944 (2012).
52. Matsuda, T. & Cepko, C. L. Controlled expression of transgenes introduced by in vivo electroporation. *Proc Natl Acad Sci USA* **104**, 1027–1032 (2007).
53. Yusa, K., Zhou, L., Li, M. A., Bradley, A. & Craig, N. L. A hyperactive piggyBac transposase for mammalian applications. *Proc Natl Acad Sci USA* **108**, 1531–1536 (2011).
54. Lyubimova, A. *et al.* Single-molecule mRNA detection and counting in mammalian tissue. *Nat Protoc* **8**, 1743–1758 (2013).
55. Yunger, S., Rosenfeld, L., Garini, Y. & Shav-Tal, Y. Quantifying the transcriptional output of single alleles in single living mammalian cells. *Nat Protoc* **8**, 393–408 (2013).

Acknowledgments

We thank Dr. Feng Zhang for providing the pTALEN_v2 (NG) vector (Addgene plasmid 32190); Dr. Robert Singer for providing the pCR4-24XMS2SL-stable vector (Addgene plasmid 31865), the pCR4-24XPP7SL (Addgene plasmid 31864), and the phage-ubc-nls-ha-tdMCP-gfp vector (Addgene plasmid 40649); Dr. Didier Trono for supplying the pLOX-TERT-iresTK vector (Addgene plasmid 12245); Dr. Connie Cepko for supplying the pCAG-Cre vector (Addgene plasmid 13775); Dr. Allan Bradley for supplying the pPB-LR5 vector; Dr. Nancy L. Craig for supplying the pCMV-hyPBase vector; Drs. Yusuke Miyanari, Ken-ichi Suzuki, Shinichi Tate, and Akinori Awazu for valuable discussions; and Ms. Noriko Sumiyoshi for technical assistance. This work was supported by Platform for Dynamic Approaches to Living System from the Ministry of Education, Culture, Sports, Science and Technology, Japan (to H.O., T. Sugawara and T.Y.), and Grants-in-Aid for Scientific Research from the Ministry of Education, Culture, Sports, Science and Technology (to H.O.).

Author contributions

H.O. designed and performed the experiments; T.Sugawara, T.Sakuma and T.Y. contributed new reagents/analytic tools; and H.O. wrote the paper.

Additional information

Supplementary information accompanies this paper at http://www.nature.com/scientificreports

Competing financial interests: The authors declare no competing financial interests.

How to cite this article: Ochiai, H., Sugawara, T., Sakuma, T. & Yamamoto, T. Stochastic promoter activation affects Nanog expression variability in mouse embryonic stem cells. *Sci. Rep.* **4**, 7125; DOI:10.1038/srep07125 (2014).

Published August 4, 2014

EDEM2 initiates mammalian glycoprotein ERAD by catalyzing the first mannose trimming step

Satoshi Ninagawa,[1,3] Tetsuya Okada,[1] Yoshiki Sumitomo,[1] Yukiko Kamiya,[3] Koichi Kato,[3,4] Satoshi Horimoto,[1] Tokiro Ishikawa,[1] Shunichi Takeda,[2] Tetsushi Sakuma,[5] Takashi Yamamoto,[5] and Kazutoshi Mori[1]

[1]Department of Biophysics, Graduate School of Science, and [2]Department of Radiation Genetics, Graduate School of Medicine, Kyoto University, Kyoto 606-8502, Japan
[3]Institute for Molecular Science and Okazaki Institute for Integrative Bioscience, National Institutes of Natural Sciences, Okazaki 444-8787, Japan
[4]Graduate School of Pharmaceutical Sciences, Nagoya City University, Nagoya 467-8603, Japan
[5]Department of Mathematical and Life Sciences, Graduate School of Science, Hiroshima University, Hiroshima 739-8526, Japan

Glycoproteins misfolded in the endoplasmic reticulum (ER) are subjected to ER-associated glycoprotein degradation (gpERAD) in which Htm1-mediated mannose trimming from the oligosaccharide $Man_8GlcNAc_2$ to $Man_7GlcNAc_2$ is the rate-limiting step in yeast. In contrast, the roles of the three Htm1 homologues (EDEM1/2/3) in mammalian gpERAD have remained elusive, with a key controversy being whether EDEMs function as mannosidases or as lectins. We therefore conducted transcription activator-like effector nuclease–mediated gene knockout analysis in human cell line and found that all endogenous EDEMs possess mannosidase activity. Mannose trimming from $Man_8GlcNAc_2$ to $Man_7GlcNAc_2$ is performed mainly by EDEM3 and to a lesser extent by EDEM1. Most surprisingly, the upstream mannose trimming from $Man_9GlcNAc_2$ to $Man_8GlcNAc_2$ is conducted mainly by EDEM2, which was previously considered to lack enzymatic activity. Based on the presence of two rate-limiting steps in mammalian gpERAD, we propose that mammalian cells double check gpERAD substrates before destruction by evolving EDEM2, a novel-type Htm1 homologue that catalyzes the first mannose trimming step from $Man_9GlcNAc_2$.

Introduction

Proteins misfolded in the ER are degraded by the proteasome via a series of events collectively termed ER-associated degradation (Xie and Ng, 2010; Smith et al., 2011; Brodsky, 2012). Among the various pathways used, the best characterized, particularly in yeast, is ER-associated glycoprotein degradation (gpERAD) in which two-step mannose trimming from high-mannose-type oligosaccharides plays crucial roles (Molinari, 2007; Hosokawa et al., 2010a; Kamiya et al., 2012). α1,2-mannosidase Mns1 catalyzes the first step, conversion of $Man_9GlcNAc_2$ (M9) to $Man_8GlcNAc_2$ isomer B (M8B), and α1,2-mannosidase Htm1 catalyzes the second step, conversion of M8B to oligosaccharides with the α1,6-mannose exposed (Mα1,6E; Fig. 1, C and E; and see Fig. 5 A). These products are then recognized by lectin Yos9 for subsequent disposal (Quan et al., 2008).

The mammalian ER expresses ER mannosidase I (ERmanI) as the sole homologue of Mns1, but expresses multiple homologues of Htm1, namely, EDEM1, EDEM2, and EDEM3 (Fig. 1, A and B). The exact roles of all these proteins in mammalian gpERAD have remained elusive. Overexpression and biochemical experiments indicated that ERmanI converted M9 to M8B (Gonzalez et al., 1999; Hosokawa et al., 2003). Overexpression of EDEM1 or EDEM3 but not EDEM2 promoted mannose trimming at various steps, including the second step (Hosokawa et al., 2003, 2010b; Mast et al., 2005; Hirao et al., 2006; Olivari et al., 2006). These results pointed to ERmanI as the first-step enzyme and to EDEM1 and EDEM3 as the second-step enzymes, and suggested that EDEM2 lacks α-mannosidase activity. However, this was puzzling to us because it had originally been proposed that EDEM1 has no α1,2-mannosidase activity (Hosokawa et al., 2001) and because it was also suggested that ERmanI is involved in the formation of $Man_{7\text{-}5}GlcNAc_2$

Correspondence to Kazutoshi Mori: mori@upr.biophys.kyoto-u.ac.jp
Y. Kamiya's present address is Graduate School of Engineering and EcoTopia Science Institute, Nagoya University, Nagoya 464-8603, Japan.

Abbreviations used in this paper: ERmanI, ER mannosidase I; gpERAD, ER-associated glycoprotein degradation; KO, knockout; M9, $Man_9GlcNAc_2$; M8B, $Man_8GlcNAc_2$ isomer B; Mα1,6E, α1,6-mannose exposed; PA, pyridylaminated; TALEN, transcription activator-like effector nuclease; WT, wild-type.

Supplemental Material can be found at:
http://jcb.rupress.org/content/suppl/2014/07/31/jcb.201404075.DC1.html

The Rockefeller University Press $30.00
J. Cell Biol. Vol. 206 No. 3 347–356
www.jcb.org/cgi/doi/10.1083/jcb.201404075

Published August 4, 2014

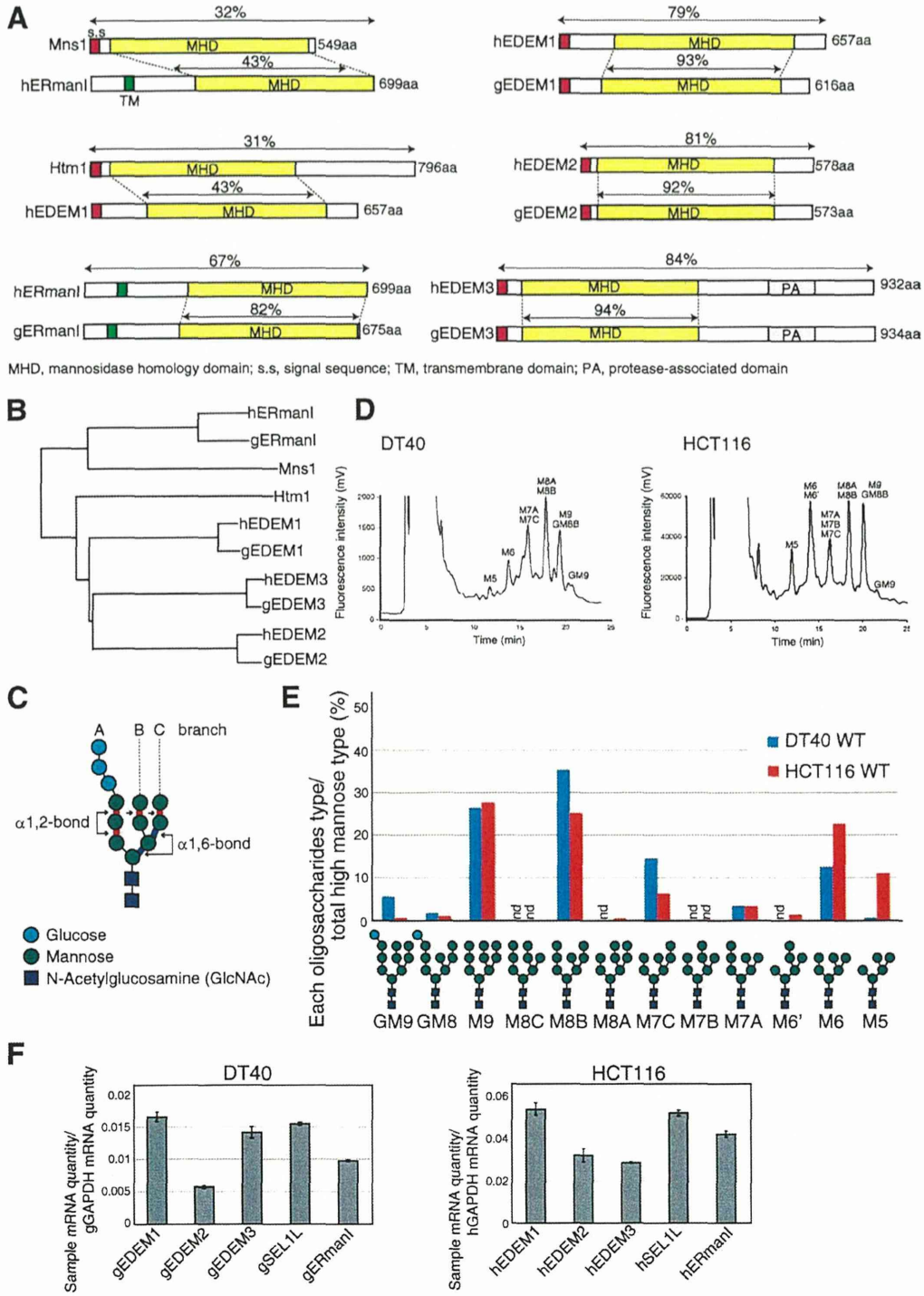

Figure 1. **Characterization of DT40 and HCT116 cell lines in regard to gpERAD.** (A) Schematic structures of yeast Mns1 and Htm1 and their homologues in chickens (g) and humans (h). Sequence identities are shown as percentages. (B) Phylogenic tree calculated by the neighbor-joining method. (C) Schematic structure of $Glc_3Man_9GlcNAc_2$. (D) Elution profiles of *N*-glycans prepared from total cellular glycoproteins of WT DT40 and HCT116 cells. This experiment was completed once. (E) Isomer composition of *N*-glycans obtained from D. nd, not detected. (F) Endogenous mRNA levels encoding chicken and human EDEM1, EDEM2, EDEM3, SEL1L, and ERmanI relative to chicken and human GAPDH mRNA level, respectively, expressed in WT DT40 or HCT116 cells ($n = 3$).

Published August 4, 2014

with Mα1,6E, based on the results of overexpression (Hosokawa et al., 2003), knockdown (Avezov et al., 2008), and biochemistry (Aikawa et al., 2012). Moreover, the finding that EDEM1 recognized not only misfolded glycoproteins but also misfolded nonglycoproteins and delivered them to the ER membrane for destruction by binding to the carbohydrate moiety of its downstream component SEL1L (Cormier et al., 2009) generated controversy as to whether EDEMs function as α1,2-mannosidases for mannose trimming or as lectins for substrate delivery (Tamura et al., 2010). We have therefore conducted gene knockout (KO) analyses in chicken and human cell lines to resolve this controversy and to determine which proteins catalyze the two key steps of mannose trimming in mammalian gpERAD.

Results and discussion

We started by determining the *N*-glycan profiles of total cellular glycoproteins prepared from wild-type (WT) DT40 cells derived from chicken B lymphocytes and HCT116 cells derived from human colonic carcinoma, both of which express Mns1 and Htm1 homologue mRNAs at comparable levels (Fig. 1 F). We focused on high-mannose-type oligosaccharides with the elution positions shown in Fig. 1 D. For comparison, Fig. 1 E shows the amount of each high-mannose-type oligosaccharide relative to the total amount of high-mannose-type oligosaccharides. M9 and M8B levels in the two cell types were comparable, consistent with the results obtained with HepG2 cells (Hosokawa et al., 2010b). In connection with this, our literature search unraveled an interesting difference between yeast and mammalian gpERAD. Namely, total *N*-glycans obtained after 10–20-min pulse labeling of yeast cells consisted almost exclusively of M8 (Clerc et al., 2009), indicating that conversion of M9 to M8B by Mns1 is highly efficient and occurs regardless of protein folding/misfolding status. Therefore, conversion of M8B to Mα1,6E by Htm1 is the initiating and rate-limiting step in yeast gpERAD (Gauss et al., 2011). In contrast, total *N*-glycans obtained after 30-min pulse labeling of HEK293 cells consisted predominantly of M9 (Hirao et al., 2006), indicating that conversion of M9 to M8B is inefficient in human cells.

We knocked out MnsI and Htm1 homologues separately in DT40 cells using homologous recombination, which is exceptionally efficient in this cell line (Fig. S1). RT-PCR showed no expression of gEDEM1, gEDEM3, or gERmanI mRNA in the respective KO cells (Fig. 2 A). Although gEDEM2-KO cells expressed some short gEDEM2 mRNAs, these mRNAs had internal deletions and therefore failed to produce any proteins when translated in vitro (Fig. S1 K). All of these KO cells grew nearly as fast as WT cells (Fig. 2 B). We determined their *N*-glycan profiles in the same way as for WT cells (Fig. S2, A and B) and identified the oligosaccharides whose contents in KO cells exceeded those in untreated WT cells. The results are shown as the increase over WT (percentage of untreated WT cells subtracted from percentage of each type of KO cell) in Fig. 2 C. When WT cells were treated with kifunensine, an inhibitor of ERmanI (Tremblay and Herscovics, 1999), M9 became predominant, as expected, but surprisingly M9 increased only slightly in gERmanI-KO cells (Fig. 2 C). This finding

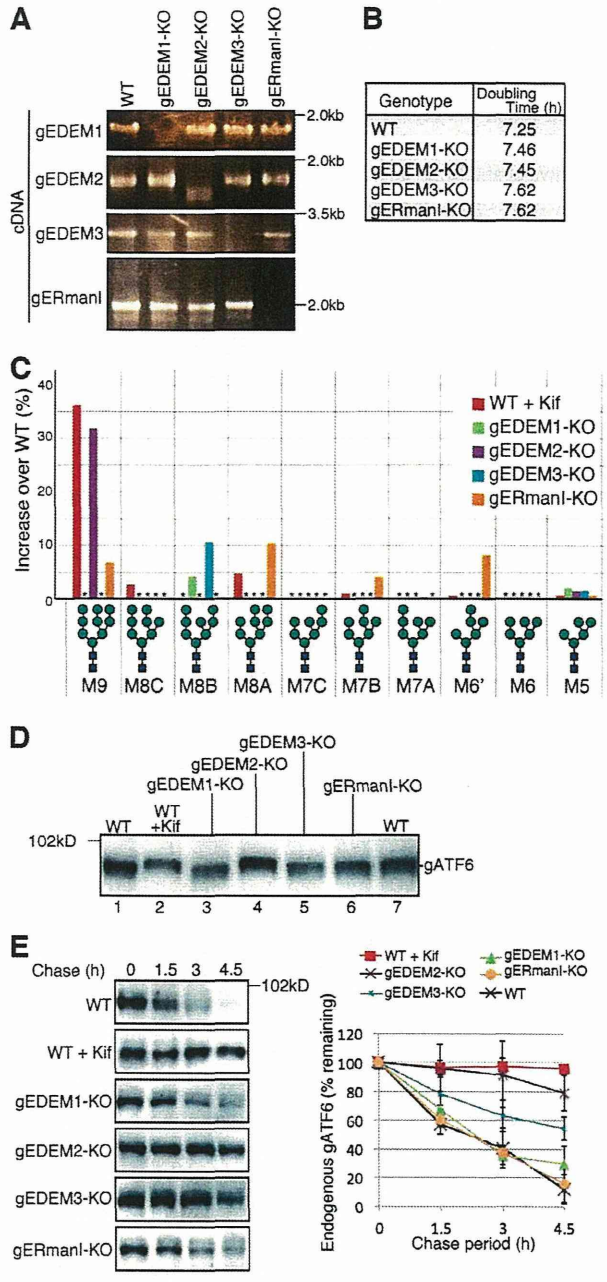

Figure 2. **Effect of gene disruption on chicken gpERAD.** (A) RT-PCR to amplify cDNA corresponding to the four α1,2-mannosidase mRNA expressed in DT40 cells of various genotypes. (B) Doubling time of WT and four α1,2-mannosidase KO cells ($n = 3$). (C) Display of oligosaccharides whose contents in kifunensine (Kif; 10 μg/ml, 6 h)-treated WT DT40 cells and four α1,2-mannosidase KO cells exceeded those in kifunensine-untreated WT cells with an increase over WT (%), as determined from isomer composition of their *N*-glycans (Fig. S2, A and B), which was completed once. Asterisks denote oligosaccharides whose contents did not exceed those in kifunensine-untreated WT cells. (D) Immunoblotting of cell lysates prepared from kifunensine-untreated or -treated WT DT40 cells and from the four α1,2-mannosidase KO cells using anti-chicken ATF6 (gATF6) antibody. (E) Cycloheximide chase to determine the degradation rate of endogenous gATF6 in kifunensine-untreated or -treated WT DT40 cells and in the four α1,2-mannosidase KO cells ($n = 3$).

Published August 4, 2014

indicates that the Mns1 homologue plays only a minor role in the conversion of M9 to M8B in DT40 cells, but is consistent with the finding that purified recombinant human ERmanI exhibited much weaker α1,2-mannosidase activity toward M9 attached to a native protein than to M9 attached to pyridylamine (Aikawa et al., 2012) and may be correlated with the unexpected localization of endogenous ERmanI at the Golgi apparatus (Pan et al., 2011). The fact that the levels of M8A, M7B, and M6′ also increased in gERmanI-KO cells (Fig. 2 C) indicates that gERmanI appears to trim the outermost mannose of the B branch randomly rather than to convert M9 to M8B specifically.

Contrary to our strong expectations from previous results (Mast et al., 2005), we were surprised to find that conversion of M9 to M8B was blocked as effectively in gEDEM2-KO cells as in WT cells treated with kifunensine (Fig. 2 C), indicating that the first-step mannose trimming in DT40 cells is mainly caused by gEDEM2 and that kifunensine inhibits both gERmanI and gEDEM2. In contrast, the level of M8B increased in gEDEM1-KO and gEDEM3-KO cells (Fig. 2 C), indicating that EDEM1 and EDEM3 are the second-step enzymes. These differences in *N*-glycan profiles were well reflected by the mobility in SDS-PAGE of ATF6, a type II transmembrane glycoprotein in the ER that functions as an unfolded protein response transducer (Haze et al., 1999): endogenous ATF6 migrated more slowly in kifunensine-treated WT and gEDEM2-KO cells than in other cell types (Fig. 2 D). We recently showed that ATF6 undergoes gpERAD in DT40 cells (Horimoto et al., 2013). Because its degradation by the proteasome is completely blocked by kifunensine treatment, it is a highly suitable substrate to determine the effect on gpERAD. Cycloheximide chase clearly showed that degradation of endogenous ATF6 occurred normally in gERmanI-KO cells, whereas it was most effectively blocked in kifunensine-treated WT and gEDEM2-KO cells (Fig. 2 E), as expected from the *N*-glycan profiles.

We then knocked out three EDEMs in the human HCT116 diploid cell line (Ochiai et al., 2014) using the transcription activator-like effector nuclease (TALEN) method (Joung and Sander, 2013). Specifically, we used the recently developed Platinum TALEN technology, which appears to have higher activity than previously reported methods (Sakuma et al., 2013). Single introduction of Platinum TALEN designed to cleave within exon 1 encoding the signal sequence of hEDEM1, hEDEM2, or hEDEM3, together with the respective targeting vector containing positive and negative selection markers, produced homo-KOs with efficiency of 20%, 19%, or 45%, respectively, and the ampicillin-resistance gene for *Escherichia coli* selection and the diphtheria toxin-A fragment gene were not incorporated into the genome when correctly targeted (Fig. 3, A and B). Genomic PCR (Fig. 3 C) and Southern blot hybridization (Fig. S3, A–D) showed incorporation of the drug-resistance gene at the expected locus in each case (four probes we tested did not work for hEDEM1 Southern blot hybridization), and RT-PCR revealed no expression of hEDEM1, hEDEM2, or hEDEM3 mRNA in the respective KO cells (Fig. 3 D). These KO cells grew as fast as WT cells (Fig. 3 E). Immunoblotting showed that ER stress marker proteins BiP, ATF4, and XBP1(S) were not induced in these KO cells (Fig. S3 E). The *N*-glycan profiles (Fig. S3, F and G) revealed that conversion of M9 to M8B was blocked in hEDEM2-KO cells as effectively as in kifunensine-treated WT HCT116 cells and that the level of M8B increased in hEDEM1-KO and hEDEM3-KO cells (Fig. 3 F). Thus, all endogenous hEDEMs function as α1,2-mannosidases. Endogenous human ATF6α migrated more slowly in kifunensine-treated WT and hEDEM2-KO cells than in untreated WT cells (Fig. 3 G), and this difference was lost after treatment with endoglycosidase H, as expected (Fig. 3 H). This difference in migration was also observed in different KO strains (Fig. S3 H). ATF6α in hEDEM3-KO cells appeared to migrate with a speed between that in untreated WT and hEDEM2-KO cells (Fig. 3 G), reflecting the marked increase in M8B level (Fig. 3 F). Degradation of endogenous ATF6α was blocked in WT HCT116 cells treated with MG132 or kifunensine, as expected, and was most effectively blocked in hEDEM2-KO cells (Fig. 4 A).

The enzymatic activity of Mns1 is strongly dependent on the EF hand motif in the mannosidase homology domain, and mutation of the glutamic acid within it (Fig. 4 B, red circle) is known to cause inactivation (Lipari and Herscovics, 1999). Importantly, when myc-tagged hATF6α (full length; Fig. 4 C, top) or hATF6α(C)-BACE(TM)-TAP (Horimoto et al., 2013; a shorter, artificial yet functional transmembrane protein containing the luminal region of hATF6α and the transmembrane region of BACE501, which is subjected to gpERAD; Fig. 4 C, bottom) was cotransfected with Flag-tagged hEDEM2 in hEDEM2-KO cells, these proteins migrated in SDS-PAGE at the same positions as in WT cells (Fig. 4 D). In contrast, no such rescue effect was observed with Flag-tagged mutant hEDEM2-E117Q (Fig. 4 D). These differences in migration were also observed for endogenous hATF6α in WT cells and hEDEM2-KO cells stably expressing Flag-tagged hEDEM2 or hEDEM2-E117Q (Fig. 4 E). Most importantly, stable introduction of Flag-tagged hEDEM2, but not Flag-tagged hEDEM2-E117Q, into hEDEM2-KO cells restored degradation of endogenous hATF6α (Fig. 4 F).

The mechanism of mammalian gpERAD was originally proposed based on the results of yeast genetics and biochemistry and overexpression in mammalian cells. However, here our pioneering application of TALEN to dissect and identify the functions of multigene family members (EDEMs) in human cells revealed that the roles of Mns1 and Htm1 homologues in mammalian gpERAD are completely discordant with those in that earlier proposed mechanism. The Mns1 homologue ERmanI plays a minor role in the conversion of M9 to M8B, the first step of gpERAD, unlike in yeast, whereas the previously passed-over Htm1 homologue EDEM2 most surprisingly plays a major role (Fig. 5 B).

We found that although hEDEM1 appeared to possess the weakest α1,2-mannosidase activity among the three hEDEMs (Fig. 3 F), deletion of hEDEM1 significantly delayed the degradation of hATF6α (Fig. 4 A). These observations are consistent with previous studies on EDEM1 (Hosokawa et al., 2010b; Ron et al., 2011; Shenkman et al., 2013). We also found that overexpression of both WT hEDEM1 and enzymatically inactive mutant hEDEM1-E225Q enhanced degradation of hATF6α(C)-BACE (TM)-TAP (Fig. S3 I). This suggests that hEDEM1 can function in gpERAD independently of its α1,2-mannosidase activity, when overexpressed or up-regulated by the unfolded protein response

Published August 4, 2014

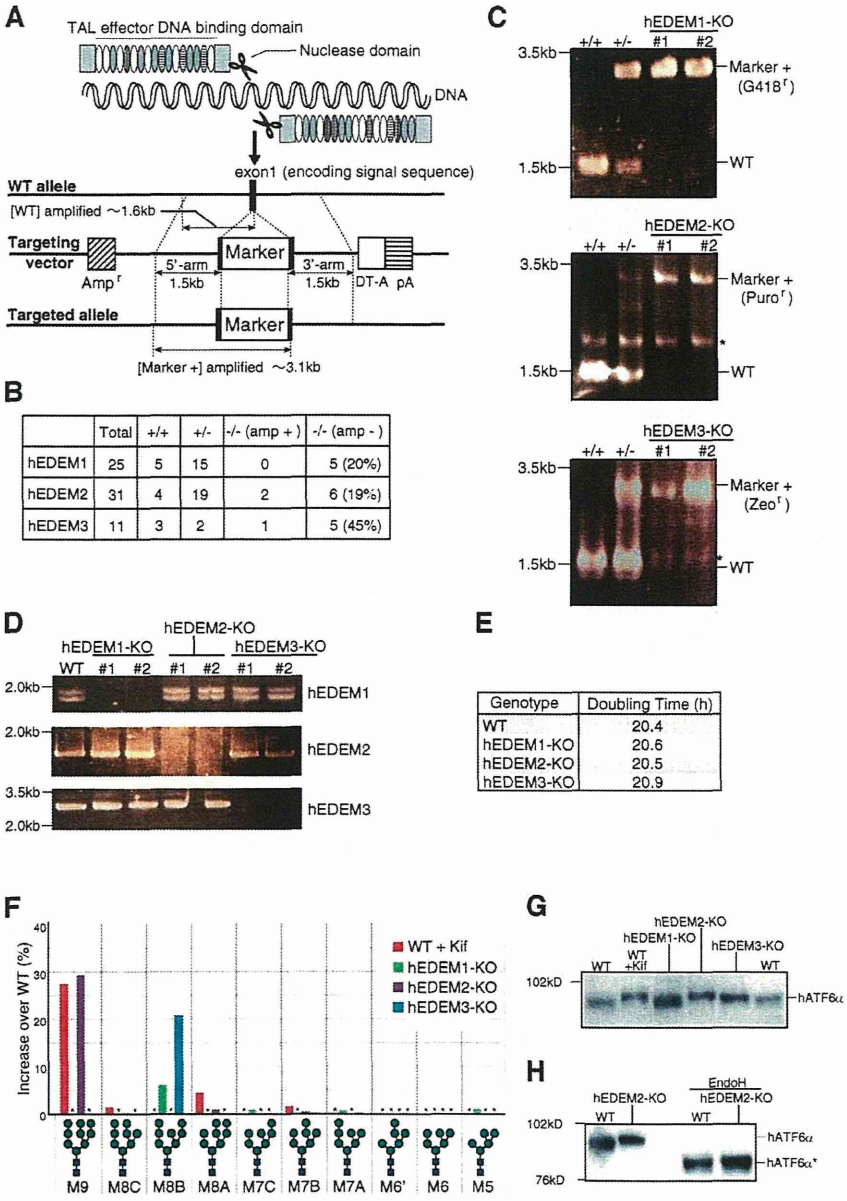

	Total	+/+	+/-	-/- (amp +)	-/- (amp -)
hEDEM1	25	5	15	0	5 (20%)
hEDEM2	31	4	19	2	6 (19%)
hEDEM3	11	3	2	1	5 (45%)

Genotype	Doubling Time (h)
WT	20.4
hEDEM1-KO	20.6
hEDEM2-KO	20.5
hEDEM3-KO	20.9

Figure 3. **Effect of gene disruption on human gpERAD.** (A) Strategy for TALEN-mediated gene disruption. Cleavage of the exon 1 encoding the signal sequence of human EDEM1, EDEM2, or EDEM3 with the designed TALEN facilitates subsequent homologous recombination with the respective targeting vector containing both positive and negative selection markers. (B) Results of screening. The presence (amp +) or absence (amp −) of the ampicillin-resistance gene in targeted alleles was checked by genomic PCR. (C) Genomic PCR to confirm homologous recombination in HCT116 cells of various genotypes. Asterisks denote nonspecific bands. (D) RT-PCR to amplify cDNA corresponding to hEDEM1, hEDEM2, or hEDEM3 mRNA expressed in HCT116 cells of various genotypes. The full-length cDNA and cDNA lacking the exon 6 were amplified as hEDEM1. (E) Doubling time of WT and three hEDEM-KO cells (n = 4). (F) Display, similarly to Fig. 2 C, of oligosaccharides whose contents in kifunensine (Kif; 10 µg/ml, 12 h)-treated WT HCT116 and three hEDEM-KO cells exceeded those in kifunensine-untreated WT cells with an increase over WT (%), as determined from isomer composition of their N-glycans (Fig. S3, F and G), which was completed once. Asterisks denote oligosaccharides whose contents did not exceed those in kifunensine-untreated WT cells. (G) Immunoblotting of cell lysates prepared from kifunensine-untreated or -treated WT HCT116 cells and from three hEDEM-KO cells using anti-human ATF6α (hATF6α) antibody. (H) Immunoblotting of cell lysates prepared from WT and hEDEM2-KO HCT116 cells with or without endoglycosidase H treatment. hATF6α* denotes the nonglycosylated hATF6α.

during ER stress (Yoshida et al., 2003), likely as a lectin for substrate delivery as proposed previously (Cormier et al., 2009).

The results obtained with TALEN-based KO in human cells are consistent with those we obtained here with conventional KO in chicken cells, demonstrating the reliability of TALEN technology. Particularly in human cells, the summation of the increase of M8B levels in hEDEM1-KO and hEDEM3-KO cells was nearly identical to the increase in M9 level in hEDEM2-KO cells (Fig. 3 F), indicating that conversion of M8B to Mα1,6E, the second step, is performed mainly by hEDEM3 and to a lesser extent by hEDEM1, not by hEDEM2. In connection with this subject, it was recently shown that SEL1L, a partner protein of the E3 ligase HRD1 spanning the ER membrane, binds to EDEM1 and EDEM3 but not to EDEM2 (Saeed et al., 2011; confirmation in Fig. S3 J). These results are consistent with our placement of EDEM1 and EDEM3 downstream of EDEM2 (Fig. 5 B).

Nonetheless, conversion of M9 to M8B by hEDEM2 is much slower than that by yeast Mns1 because M9 and M8B exist at comparable levels in human cells (Fig. 1 E). In other words, mammalian gpERAD has two rate-limiting steps in mannose trimming. As overexpression of hEDEM2 or hEDEM3 did not affect the level of hATF6α(C)-BACE(TM)-TAP (Fig. S3 I), the expression levels of EDEM2 or EDEM3 are not the primary determinants of the speed of mannose trimming. Interestingly, it was recently shown that EDEM1 and EDEM2 bind to ricin A chain, which is retrotranslocated from the ER to the cytosol similarly to ERAD substrates, but they bind much less efficiently to its P250A mutant, which is less hydrophobic than the WT (Sokołowska et al., 2011; Słomińska-Wojewódzka et al., 2014),

Published August 4, 2014

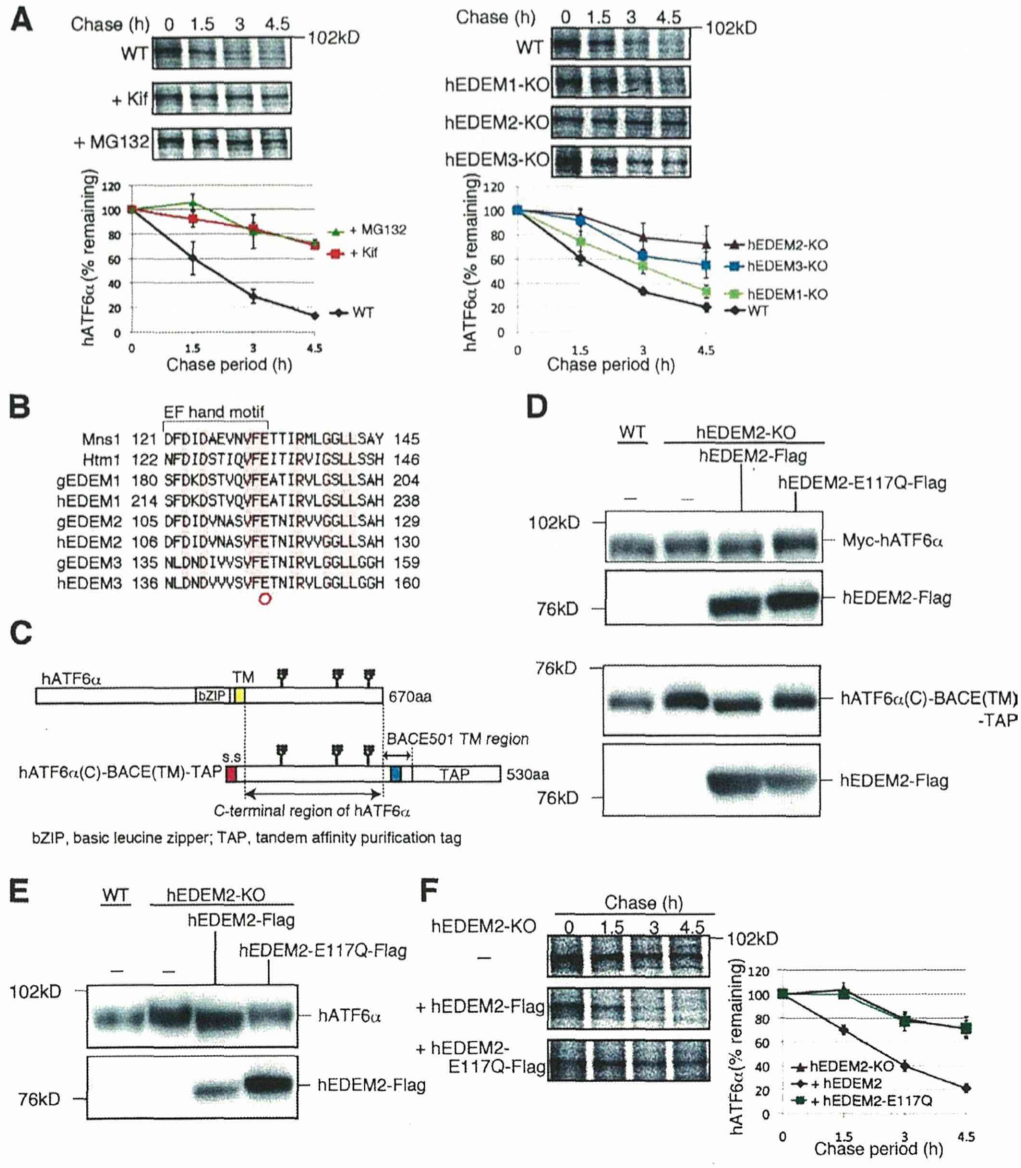

Figure 4. **Requirement for α1,2-mannosidase activity of hEDEM2 in human gpERAD.** (A) Pulse chase to determine the degradation rate of endogenous hATF6α in WT HCT116 cells with or without kifunensine or MG132 treatment and in three hEDEM-KO cells ($n = 3$). (B) Alignment of amino acid sequences around the EF hand motif, which is essential for the α1,2-mannosidase activity of Mns1, with those of Htm1 and their homologues in chicken and human. Identical amino acids are highlighted. (C) Schematic structure of hATF6α and hATF6α(C)-BACE(TM)-TAP. Potential *N*-glycosylation sites are shown schematically. (D) Immunoblotting of cell lysates prepared from WT and hEDEM2-KO HCT116 cells in which Myc-hATF6α (top) or hATF6α(C)-BACE(TM)-TAP (bottom) was expressed by transfection together with hEDEM2-Flag or hEDEM2-E117Q-Flag, using anti–c-myc and anti-Flag antibodies. (E) Immunoblottig of cell lysates prepared from WT HCT116, hEDEM2-KO, and hEDEM2-KO cells stably expressing hEDEM2-Flag or hEDEM2-E117Q-Flag using anti-human ATF6α and anti-Flag antibodies. (F) Pulse chase to determine the degradation rate of endogenous hATF6α in HCT116 hEDEM2-KO and hEDEM2-KO cells stably expressing hEDEM2-Flag or hEDEM2-E117Q-Flag ($n = 3$).

suggesting that they recognize not only sugar structures but also protein structures.

Taking the aforementioned findings all together we propose that mammalian cells double check gpERAD substrates by evolving a novel-type Htm1 homologue that catalyzes the first mannose trimming step from M9 and thereby expressing three EDEMs with different specificity for glycoprotein folding/misfolding, first by EDEM2 (for conversion of M9 to M8B) and then by EDEM1/3 (for conversion of M8B to Mα1,6E), before recognition by lectin OS-9 (Fig. 5 B). This is more sophisticated than single check by Htm1 in yeast cells, as it avoids the unnecessary destruction of proteins, whose synthesis is energy expensive, and allows the escape of folded proteins from ERAD.

Materials and methods

Construction of plasmids

Recombinant DNA techniques were performed according to standard procedures (Sambrook et al., 1989) and the integrity of all constructed

Published August 4, 2014

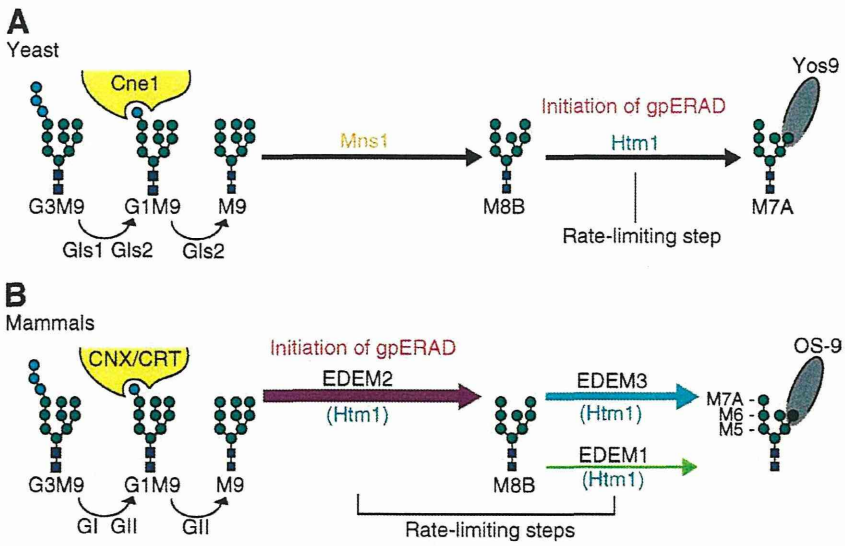

Figure 5. **Models of yeast and mammalian gpERAD.** (A) In yeast, high-mannose-type oligosaccharide attached to asparagine ($Glc_3Man_9GlcNAc_2$, G3M9) is first trimmed to M9 by glucosidases Gls1 and Gls2. M9 is trimmed to M8B by Mns1 and M8B is trimmed to M7A by Htm1. G1M9 is recognized by lectin chaperone Cne1 for folding, whereas M7A exposing α1,6-mannose is recognized by lectin Yos9 for subsequent degradation. The rate-limiting step in yeast gpERAD is the trimming from M8B to M7A. Refer to reviews by Molinari (2007) and Hosokawa et al. (2010a). (B) In mammals, G3M9 is trimmed to M9 by glucosidase I (GI) and glucosidase II (GII), homologues of yeast Gls1 and Gls2, respectively. G1M9 is recognized by lectin chaperones calnexin (CNX) and calreticulin (CRT), homologues of yeast Cne1, for folding. As our current results unambiguously show that M9 is mainly trimmed to M8B by EDEM2 and that M8B is trimmed by EDEM1 and EDEM3 to $Man_{7\text{-}5}GlcNAc_2$, which are recognized by lectin OS-9, a homologue of yeast Yos9, for degradation, mammalian gpERAD has two rate-limiting steps.

plasmids was confirmed by extensive sequencing analyses. Site-directed mutagenesis was performed using DpnI. p3*flag-CMV™-14 expression vector (Sigma-Aldrich) was used to express a protein tagged with Flag at the C terminus. Platinum TALEN plasmids were constructed as described previously (Sakuma et al., 2013). In brief, each DNA-binding module was assembled into ptCMV-136/63-VR vectors using the two-step Golden Gate cloning method. Assembled sequences were 5′-TGGCGAGCGCTC-GTCCTGgggctggtgctcctcCGGCTTGGCCTCCATGGA-3′ for hEDEM1, 5′-TCCGGCTGCTCATCCCGctcggcctcctgtgcGCGCTGCTGCCTCAGCA-3′ for hEDEM2, and 5′-TGTGGGTCCCCGGTTCCcagcgagcgcgatgGAGAC-TAGTGGCGGCGA-3′ for hEDEM3, where uppercase and lowercase letters indicate TALEN target sequences and spacer sequences, respectively.

Cell culture and transfection

DT40 cells were cultured and transfected as described previously (Ninagawa et al., 2011). HCT116 cells (CCL-247; ATCC) were cultured in Dulbecco's modified Eagle's medium (4.5 g/l glucose) supplemented with 10% fetal bovine serum, 2 mM glutamine, and antibiotics (100 U/ml penicillin and 100 µg/ml streptomycin) at 37°C in a humidified 5% CO_2/95% air atmosphere. Transfection was performed using Lipofectamine 2000 (Invitrogen) according to the manufacturer's instructions. HCT116 cells stably expressing hEDEM2-Flag or hEDEM2-E117Q-Flag from p3*Flag-CMV™14 expression vector were selected after culture for 20 d in the presence of 0.6 mg/ml G418.

Analysis of *N*-glycans of total cellular glycoproteins

Pyridylamination and structural identification of *N*-glycans of total cellular glycoproteins were performed as described previously (Hosokawa et al., 2010b). In brief, *N*-glycans released from delipidated cells by hydrazinolysis were re*N*-acetylated using acetic anhydrides, and then labeled with fluorescent 2-aminopyridine (Wako Pure Chemical Industries). Pyridylaminated (PA) oligosaccharides were fractionated by HPLC first on a TSK gel Amide-80 (amide-silica) column (Tosoh) and second on a Shim-pack HRC-octadecyl silica column (Shimadzu). Elution times of individual peaks from the amide-silica and octadecyl silica columns were normalized with respect to the degree of polymerization of PA-isomalto-oligosaccharide and are represented in units of glucose. *N*-Glycan structures were identified based on their elution times from these columns in comparison with those of PA-glycans in the GALAXY database (Takahashi and Kato, 2003) and confirmed by cochromatography with standard PA-high mannose type oligosaccharides (Tomiya et al., 1991; Kamiya et al., 2008).

Reagents

Puromycin (0.5 µg/ml), histidinol (1 mg/ml), mycophenolic acid (15 µg/ml), blasticidin S (25 µg/ml), G418 (2 mg/ml for DT40 and 0.6 mg/ml for HCT116), and zeocin (1 mg/ml) were used for the selection and maintenance of drug-resistant clones. Kifunensine was purchased from Cayman Chemical Company; endoglycosidase H from EMD Millipore; cycloheximide from Sigma-Aldrich; MG132 from Peptide Institute; and Z-VAD-fmk from Promega.

Immunological techniques

Immunoblotting analysis was performed according to the standard procedure (Sambrook et al., 1989) as described previously (Ninagawa et al., 2011). Chemiluminescence obtained using Western blotting Luminol Reagent (Santa Cruz Biotechnology, Inc.) was detected using an LAS-3000mini LuminoImage analyzer (Fujifilm). Rabbit anti–chicken ATF6 (Horimoto et al., 2013) and rabbit anti–human ATF6α (Haze et al., 1999) antibodies were raised previously. Mouse anti–c-myc antibody (9E10) was obtained from Wako Pure Chemical Industries; mouse anti-Flag antibody from Sigma-Aldrich; mouse anti-KDEL antibody from Medical and Biological Laboratories; rabbit anti–human ATF4 and rabbit anti–mouse XBP1 antibodies from Santa Cruz Biotechnology, Inc.; and rabbit anti–human GAPDH from Trevigen. Rabbit anti–human SEL1L antibody was a gift from N. Hosokawa (Kyoto University, Kyoto, Japan).

Pulse-chase experiments and subsequent immunoprecipitation were performed according to procedures described previously (Ninagawa et al., 2011). After incubation for 30 min in methionine- and cysteine-free Dulbecco's modified Eagle's medium (Invitrogen) supplemented with 2 mM glutamine and 10% dialyzed fetal bovine serum, cells were pulse labeled with 2.0 Mbq/dish EXPRE^{35}S^{35}S protein labeling mixture (PerkinElmer) and then chased in fresh complete medium. Cells were lysed in buffer A (50 mM Tris/Cl, pH 8.0, containing 1% NP-40, 150 mM NaCl, protease inhibitor cocktail (Nacalai), 20 µM MG132, and 2 µM Z-VAD-fmk). Immunoprecipitation was performed using anti-hATF6α antibody and protein A–coupled Sepharose beads (GE Healthcare). Beads were washed with high salt buffer (50 mM Tris/Cl, pH 8.0, containing 1% NP-40 and 150 mM NaCl) twice, washed with PBS, and heated at 65°C in Laemmli's sample buffer. Immunoprecipitates were subjected to SDS-PAGE, and radioactive bands were analyzed using a FLA-3000G FluoroImage analyzer (Fujifilm).

Quantitative RT-PCR

Quantitative RT-PCR was performed using the SYBR Green method (Applied Biosystems) using a pair of primers, namely, 5′-CTGCACATGGCT-CATGACCTA-3′ and 5′-ACCCGAGGATACGGAATTCC-3′ for gEDEM1, 5′-CTGAAGGCACTGTGGAAAAACC-3′ and 5′-GCCACCCATTTGGC-AGTTAC-3′ for gEDEM2, 5′-GCGCAGCAGCAATTTGGT-3′ and 5′-CC-GCTCCAACTCCACTATCTTT-3′ for gEDEM3, 5′-TTTGGTGTGCAACAA-CCTATG-3′ and 5′-CCTCTTATTGGACTGCTCTTCA-3′ for gSEL1L, 5′-AGT-GCCAAGATGGATCACTTG-3′ and 5′-TGATCAGCAGTCAATCCATTG-3′ for gERmanI, 5′-CTGATGCCCCCATGTTTGTG-3′ and 5′-GCACGATGCATTGCTG-ACA-3′ for gGAPDH, 5′-AGTTCCTCCTGACACCAATA-3′ and 5′-GTCGACT-CAGAATCCCAAAT-3′ for hEDEM1, 5′-CGCTTCGATGACTGGTACCT-3′ and 5′-TAGGCCTCCAAGGACTGGAA-3′ for hEDEM2, 5′-ATTAGCCAGC-CACCTCTTCT-3′ and 5′-AGCAAAGCATCCATCCAAGT-3′ for hEDEM3, 5′-GGTTTGGCACCGATGTAGAT-3′ and 5′-AGCTTGTGCACTGTGTTGCT-3′

Published August 4, 2014

for hSEL1L, 5′-CCCGAGCCTAGGGACAAGAT-3′ and 5′-CCCGAGCCTAGGGACAAGAT-3′ for hERmanI, or 5′-GACCCCTTCATTGACCTCAA-3′ and 5′-TTGACGGTGCCATGGAATT-3′ for hGAPDH. 2,000, 8,000, 20,000, 80,000, and 200,000 molecules of plasmid carrying the respective gene were used as standards.

Southern blot hybridization

Southern blot hybridization was performed according to standard procedures (Sambrook et al., 1989) as described previously (Ninagawa et al., 2011). Specific probes were amplified by PCR from DT40 cell genomic DNA using the primers 5′-TGAAACTTGCACTGCAGGAG-3′ and 5′-ACCCCCTTCGTAAGTGGTTC-3′ for gEDEM1, 5′-GAAGGCTCTGAAGGCACTGT-3′ and 5′-TGTCGGATCCCTTTCAACTC-3′ for gEDEM2, 5′-AGCCGATTCACAGGAACATC-3′ and 5′-AAGAAGGGCAGTGCACAAAT-3′ for gEDEM3, or 5′-AAATTATTCTGATGCACATG-3′ and 5′-CTCTTGTATGCATCGATATGf-3′ for gERmanI, or from HCT116 cell genomic DNA using the primers 5′-CCACTGACCCTAACAATTGC-3′ and 5′-AAATGAGGCAAAGTAATGCC-3′ for hEDEM2 and 5′-GGTCACTTGATGGAAAAAAGC-3′ and 5′-ATTTGGTTGAACTTTTCCAG-3′ for hEDEM3. These probes were labeled with digoxigenin. Subsequent reaction with anti-digoxigenin antibody (Roche) and treatment with the chemiluminescent detection reagent CDP-star (GE Healthcare) were performed according to the manufacturer's specifications. Chemiluminescence was visualized using an LAS-3000mini LuminoImage analyzer.

Genomic PCR

Homologous recombination in HCT116 cells was confirmed by genomic PCR using a pair of primers: 5′-CTATGTGCCAGCTACCATGTG-3′ and 5′-TACTCCATGGAGGCCAAGCC-3′ for hEDEM1, 5′-CCCCAGGGTAGTCATTTGTC-3′ and 5′-ATCTGGCGCGGAGCCGTCGG-3′ for hEDEM2, or 5′-GAGTACAGAGAGAAAAAGGAC-3′ and 5′-GCCACTAGTCTCCATCGCGC-3′ for hEDEM3. The presence of the ampicillin-resistance gene in targeted alleles was checked by genomic PCR using a pair of primers: 5′-GAGCACTTTTAAAGTTCTGC-3′ and 5′-TTACCAATGCTTAATCAGTG-3′.

RT-PCR

Total RNA prepared from WT DT40 cells or various KOs (~5 × 10^6 cells) and from WT HCT116 cells or various KOs (~3 × 10^6 cells) by the acid guanidinium/phenol/chloroform method using ISOGEN (Nippon Gene) was converted to cDNA using Moloney murine leukemia virus reverse transcription (Invitrogen) and random primers. Full-length open reading frame of gEDEM1, gEDEM2, gEDEM3, gERmanI, hEDEM1, hEDEM2, or hEDEM3 was amplified using PrimeSTAR HS DNA polymerase (Takara Bio Inc.) and a pair of primers, namely, 5′-GGGTACCATGCAATGGCGCTCGCTGGT-3′ and 5′-CTCTAGAGATCAAGCCCACCATCCGAT-3′ for gEDEM1, 5′-GGAATTCACCATGGCGCTGCTGCGCTCGCT-3′ and 5′-GCAGATCTGGAGTGTTGTCCAGGAAGACCT-3′ for gEDEM2, 5′-GGAATTCACCATGGGCGGAGCTGCGGGCTG-3′ and 5′-CTATCGATGGTAGTTCATCCTTTTCCATCA-3′ for gEDEM3, 5′-GAAGATCTCGCCATGTACGCTGCCGCCGCC-3′ and 5′-GCTCTAGATGCTGGCACCCAGATGGGGAG-3′ for gERmanI, 5′-GAAGATCTGACCATGCAATGGCGAGCGCTC-3′ and 5′-CGGGATCCAATCAAACCAACCATCTGGTC-3′ for hEDEM1, 5′-CCCAAGCTTGCTCTATGCCTTTCCGGCTGC-3′ and 5′-GCTCTAGATGAGGAGTCTAGGAAAACCTG-3′ for hEDEM2, or 5′-GAAGATCTGGCCATGAGCGAAGCCGGCG-3′ and 5′-CGGGATCCTAGCTCATCCTTCTCCATCA-3′ for hEDEM3.

In vitro translation

In vitro translation was performed using the TNT Quick Coupled Transcription/Translation Systems (Promega) and EASY TAG EXPRESS Protein labeling mix [^{35}S] (PerkinElmer) according to the manufacturer's instructions. Translated proteins were subjected to SDS-PAGE (12% gel) and radiolabeled proteins were visualized using an FLA-3000G FluoroImage analyzer.

Construction of gEDEM1 targeting vector

The 3.6-kb fragment of the gEDEM1 gene used for the 5′ arm was amplified by PCR from DT40 cell genomic DNA using the primers 5′-CCTCGAGTGGAGCTGTACCTGCTGTTG-3′ and 5′-CGGATCCGTAGCTGTCGTAGCCGAAGG-3′, and then subcloned between the XhoI and BamHI sites of pBluescript II KS (+) vector to create the pBluescript-5′ arm (gEDEM1). The 2.3-kb fragment of the gEDEM1 gene used for the 3′ arm was amplified similarly using the primers 5′-CCGGATCCGGGAAATTCTTCCGAGTTCC-3′ and 5′-CCCTCGAGGGAACTCCCTTCTTCAGGTTG-3′, and then subcloned between the BamHI and NotI sites of the pBluescript-5′ arm (gEDEM1) to create the pBluescript-5′-3′ arms (gEDEM1). The puromycin-resistance gene flanked by loxP sites designated Puro-loxP or histidinol-resistance (histidinol dehydrogenase [HisD]) gene was subcloned into the BamHI site of the pBluescript-5′-3′ arms (gEDEM1) to create pKO-gEDEM1-puromycin or pKO-gEDEM1-histidinol, respectively (Fig. S1 A). These constructs were transfected into DT40 cells by electroporation after linearization using SacI.

Construction of gEDEM2 targeting vector

The 3.2-kb fragment of the gEDEM2 gene used for the 5′ arm was amplified by PCR from DT40 cell genomic DNA using the primers 5′-GGACTAGTTAGCAGCAGGAGACCCTTGT-3′ and 5′-CGGGATCCGCTCGTAGGCGTGGTAGAAC-3′, and then subcloned between the SpeI and BamHI sites of pBluescript II KS (+) vector to create the pBluescript-5′ arm (gEDEM2). The 2.4-kb fragment of the gEDEM2 gene used for the 3′ arm was amplified similarly using the primers 5′-CGGGATCCGCAATGTCACCGAGTTCCAG-3′ and 5′-CCCTCGAGACCAATCCCAGCAGTACAGG-3′, and then subcloned between the BamHI and XhoI sites of the pBluescript-5′ arm (gEDEM2) to create the pBluescript-5′-3′ arms (gEDEM2). The neomycin-resistance gene flanked by loxP sites designated Neo-loxP or blasticidin S-resistance gene flanked by loxP sites designated Bsr-loxP was subcloned into the BamHI site of the pBluescript-5′-3′ arms (gEDEM2) to create pKO-gEDEM2-neomycin or pKO-gEDEM2-blasticidin S, respectively. HisD was also subcloned into the BamHI site of the pBluescript-5′-3′ arms (gEDEM2) to create pKO-gEDEM2-histidinol (Fig. S1 D). These constructs were transfected into DT40 cells by electroporation after linearization using SpeI or ScaI.

Construction of gEDEM3 targeting vector

The 2.2-kb fragment of the gEDEM3 gene used for the 5′ arm was amplified by PCR from DT40 cell genomic DNA using the primers 5′-CGAGCTCCCATGAGCAAGGAGGAGAAG-3′ and 5′-CGGGATCCTGGTCAAACATTTCCAGCAC-3′, and then subcloned between the SacI and BamHI sites of pBluescript II KS (+) vector to create the pBluescript-5′ arm (gEDEM3). The 3.4-kb fragment of the gEDEM3 gene used for the 3′ arm was amplified similarly using the primers 5′-CGGGATCCTTCTCCCTGACCTTGATTGA-3′ and 5′-CCCTCGAGAATCGGCTTAAAGCTGCAAA-3′, and then subcloned between the BamHI and XhoI sites of the pBluescript-5′ arm (gEDEM3) to create the pBluescript-5′-3′ arms (gEDEM3). The Neo-loxP was subcloned into the BamHI site of the pBluescript-5′-3′ arms (gEDEM3) to create pKO-gEDEM3-neomycin. The HisD or mycophenolic acid–resistance gene, designated *E. coli* xanthine-guanine phosphoribosyltransferase (EcoGPT), was also subcloned into the BamHI site of the pBluescript-5′-3′ arms (gEDEM3) to create pKO-gEDEM3-histidinol or pKO-gEDEM3-mycophenolic acid, respectively (Fig. S1 G). These constructs were transfected into DT40 cells by electroporation after linearization using PvuI or SacI.

Construction of gERmanI targeting vector

The 3.6-kb fragment of the gERmanI gene used for the 5′ arm was amplified by PCR from DT40 cell genomic DNA using the primers 5′-ATAAGAATGCGGCCGCACATGAACACTGAACTGCTG-3′ and 5′-CGGGATCCGCTTCCATTTCTTCCAGAGAG-3′, and then subcloned between the NotI and BamHI sites of pBluescript II KS (+) vector to create the pBluescript-5′ arm (gERmanI). The 2.8-kb fragment of the gERmanI gene used for the 3′ arm was amplified similarly using the primers 5′-CCATCGATGACTACCCAGAGCTTTCACC-3′ and 5′-CCGCTCGAGCAACTCAATCAAAATTCTG-3′, and then subcloned between the ClaI and XhoI sites of the pBluescript-5′ arm (gERmanI) to create the pBluescript-5′-3′ arms (gERmanI). Neo-loxP or Puro-loxP was subcloned into the BamHI site of the pBluescript-5′-3′ arms (gERmanI) to create pKO-gERmanI-neomycin or pKO-gERmanI-puromycin, respectively (Fig. S1 L). These constructs were transfected into DT40 cells by electroporation after linearization using NotI.

Construction of gEDEM1-, gEDEM2-, gEDEM3-, and gERmanI-KO cells

Exons encoding the N-terminal region of the mannosidase homology domain of gEDEM1, gEDEM2, or gEDEM3 were replaced with one of the five drug-resistance genes (Fig. S1, A, D, and G). Homologous recombination was checked by Southern blotting (Fig. S1, B, E, and H). We obtained two independent clones (−/− #1 and #2), in which the allelic gEDEM1 genes were disrupted by HisD and Puro-loxP (Fig. S1, B and C). As RT-PCR analysis showed that gEDEM1 mRNA was not expressed in these clones (Fig. S1 J), we used −/− #1 as gEDEM1-KO (Fig. 2 A). The gEDEM2 gene is encoded in chromosome 2, which is in trisomy in DT40 cells. We thereby obtained two independent clones (−/−/− #1 and #2) in which all three alleles of the gEDEM2 gene were disrupted by Neo-loxP, HisD, and Bsr-loxP (Fig. S1, E and F). Neo-loxP and Bsr-loxP were then eliminated from their genome using the Cre-loxP system to obtain −/−/− (loxP−) #1 and #2 for further disruption (Fig. S1, E and F). RT-PCR analysis showed that these loxP− clones expressed some shorter gEDEM2 mRNAs (Fig. S1 J). Thus, gEDEM2 cDNA was amplified by RT-PCR from WT cells and gEDEM2